Characterization of atomic layer deposited semiconducting Co_3O_4

Konner E. K. Holden, and John F. Conley

Citation: Journal of Vacuum Science & Technology A **37**, 020903 (2019); doi: 10.1116/1.5064469
View online: https://doi.org/10.1116/1.5064469
View Table of Contents: https://avs.scitation.org/toc/jva/37/2
Published by the American Vacuum Society

Characterization of atomic layer deposited semiconducting Co_3O_4

Konner E. K. Holden and John F. Conley, Jr.
School of Electrical Engineering and Computer Science, Oregon State University, Corvallis, Oregon 97330

(Received 4 October 2018; accepted 14 December 2018; published 11 January 2019)

The authors report on the optical and electrical properties of atomic layer deposited (ALD) Co_3O_4 on Si, SiO_2/Si, and Co/Si substrates using $Co(Cp)_2$ and ozone. Within the ALD temperature window of 175 and 275 °C, the growth per cycle (GPC) on Si is approximately 0.050 nm/cycle. GPC is slightly lower on SiO_2 (0.043 nm/cycle) and much higher on Co substrates (0.21 nm/cycle) due to rapid ozone oxidation of Co during ALD. Grazing incidence x-ray diffraction (GIXRD) indicates a randomly oriented polycrystalline Co_3O_4 phase. The refractive index, measured using variable angle spectroscopic ellipsometry, is found to be ~2.8 within the ALD window. Optical transitions of 0.76, 1.50, and 2.22 eV are found from absorption analysis. Four-point probe measurements indicate resistivity in the range of 4.1–10.9 Ω cm. GIXRD, refractive index, optical transitions, and resistivity are all consistent with p-type semiconducting Co_3O_4. *Published by the AVS.*
https://doi.org/10.1116/1.5064469

I. INTRODUCTION

While numerous n-type semiconducting oxides, such as ZnO, In_2O_3, SnO_2, InGaZnO, and ZnSnO, have found use in a variety of important applications, relatively few p-type semiconducting oxides have been identified, including SnO, NiO, Cu_2O, and cobalt oxide.[1] Cobalt oxide exists in two stable phases, CoO and Co_3O_4. The rock-salt type CoO phase is reported to be electrically insulating with bandgap values ranging from 2.3 to 6 eV[2–4] and is of interest for metal/insulator/metal tunnel diodes in rectifying antenna (rectenna) based infrared energy harvesting.[5] The spinel-type cobalt(II,III) oxide, Co_3O_4, is an intrinsically p-type antiferromagnetic semiconductor. Owing to absorptions in the optical region, strong catalytic properties, and abundance, Co_3O_4 has attracted increasing interest for renewable energy applications in photovoltaic solar cells, photocatalysis, and Li-ion batteries.[6–9] Despite this increasing interest, the electrical and optical properties of Co_3O_4 such as resistivity, absorption coefficient, and refractive index have not been extensively reported.[8,10–18] Other properties, such as the electronic band structure and fundamental energy gap, are not fully understood and are still under debate with reported values ranging from 0.7 to 2.2 eV for bulk and thin film Co_3O_4, depending on the type of optical measurements or density functional theory (DFT) calculations performed.[7,8,10,11,13–16]

CoO and Co_3O_4 have been deposited by a variety of methods including chemical vapor deposition (CVD),[9] metal organic (MO) CVD,[10] spray pyrolysis,[8,19] pulsed CVD,[13] and atomic layer deposition (ALD).[6,12,17,18,20–26] ALD involves purge-separated, self-limiting surface chemical reactions between precursors and oxidizing agents so that the film is built up in a layer-by-layer manner. Advantages of self-limiting chemistry include atomic scale control of deposition, high uniformity, and high conformality. ALD is thus the preferred method for applications which require deposition of highly uniform and conformal films over extreme topography. To date, however, there have been relatively few reports of ALD processes for cobalt oxide (see Table I for summary) and even fewer reports on the properties of these materials. To the best of our knowledge, there are only three reports of resistivity,[12,18,25] one report of refractive index[17] and no reports of optical bandgap for ALD Co_3O_4.

In this work, we thoroughly examine the ALD process space for bis(cyclopentadienyl)cobalt(II) cobalt and ozone (O_3) and report the structural, optical, and electrical properties of the resulting cobalt oxide thin films.

II. EXPERIMENT

ALD of cobalt oxide was performed using alternating N_2-purge-separated pulses of bis(cyclopentadienyl)cobalt(II) cobalt [cobaltocene, $Co(Cp)_2$], held at 100 °C, and O_3. $Co(Cp)_2$ has a vapor pressure of 2.1 hPa at 100 °C.[27] O_3 was generated at 50% power in an AC-2025 ozone generator from IN-USA, yielding an expected O_3/O_2 concentration of ~10%. ALD was carried out in a Picosun SUNALE R-150B reactor at ~12 Torr using sequentially pulsed cycles of 0.5 s $Co(Cp)_2$/15 s N_2/3 s O_3/15 s N_2.

The optical and morphological properties of ALD films were measured on <100> Si substrates with a 1.6–2.0 nm native SiO_2 layer present. Substrates of 100 nm thermally grown SiO_2 on Si and 50 nm of thermally evaporated Co on Si were also investigated in nucleation and growth-per-cycle measurements. Film thickness, refractive index (R.I.), and extinction coefficient, used to calculate absorption coefficient, were measured using a J. A. Woollam M2000 variable angle spectroscopic ellipsometer (VASE) in the wavelength range of 300–1000 nm (1.2–4.1 eV). R.I. and extinction coefficient measurements further into the NIR were carried out with a separate VASE (Woollam V-VASE) using a multiple sample analysis technique in the wavelength range of 300–3200 nm (0.4–4.1 eV). Film crystal properties were investigated via grazing incidence x-ray diffraction (GIXRD)

Note: This paper is part of the 2019 special collection on Atomic Layer Deposition (ALD).
[a]Electronic mail: jconley@eecs.oregonstate.edu

TABLE I. Summary of ALD processes reported for cobalt oxide and associated material properties. The "phase" column lists the as-deposited phase reported using XRD or XPS analysis, followed by the phase that was obtained through annealing.

Precursor	Reactant	Temperature window (°C)	GPC (nm/cycle)	Nucleation cycles	Phase	E_{opt} (eV)	R.I.	ρ (Ω cm)	References
$Co(Cp)_2$	**~10% O_3**	**175–275**	**0.05**	**0**	**Co_3O_4**	**0.76, 1.5, 2.2**	**2.8**	**4.1–10.9**	**This work**
$Co(Cp)_2$	11% O_3	150–250	0.027	0*	Co_3O_4/CoO, Co_3O_4	—	—	—	23
$Co(Cp)_2$	15% O_3	150–280	0.045	—	Co_3O_4	—	—	—	22
$Co(Cp)_2$	O_2 plasma	100–400	0.05	0*	Co_3O_4	—	—	0.5–5.3	18 and 33
$Co(thd)_2$	O_3	114–307	0.022	0*	Co_3O_4	—	—	0.1–4.5	12 and 25
(CCTBA)	11% O_3	68–80	0.08	—	Co_3O_4/CoO	—	2.7	—	17
$CpCo(CO)_2$	11% O_3	50–150	0.08–0.11	—	Co_3O_4	—	—	—	20
$Co(dpdab)_2$	11% O_3	120–250	0.10–0.12	—	Co_3O_4	—	—	—	21
CoI_2	O_2	475–600	0.1–0.2	—	Co_3O_4	—	—	—	24
$Co^{II}(DMOCHCOCF_3)_2$	O_3	150–200	0.02	~400*	Co_3O_4[a]	—	—	—	26
$Co(^{tbu2}DAD)_2$	O_3 150 g/Nm^3	~110–120	0.12	~20*	Co_3O_4, CoO[a]	—	—	—	6

[a]Stars (*) indicate our own interpretation of the reported data. Dashes (—) indicate the absence of reported data.

using a Rigaku Ultima IV diffractometer with Cu Kα radiation (λ = 1.5406 Å). Root-mean-square (RMS) surface roughness was measured using an Asylum AFM system in air with Tap150Al-G cantilevers in AC tapping mode. Elemental analysis was performed using x-ray photoelectron spectroscopy (XPS) on a Thermo K-Alpha+ with a base pressure of 1×10^{-9} mbar and a monochromatic Al source with a spot size of 200 um with the electron flood gun on. A Jandel RM2 four-point probe was used for measuring resistivity of Co_3O_4 films deposited on an insulating (100 nm thermal SiO_2) substrate. Five measurements were taken (center and four corners) on a 1 in. × 1 in. square sample and thicknesses measured with VASE were used for resistivity calculations.

III. RESULTS AND DISCUSSION

A. ALD temperature window, nucleation, and uniformity

Shown in Fig. 1 is a plot of growth-per-cycle (GPC) versus deposition temperature for ALD films grown on a Si substrate using a 0.5/15/3/15 s pulse sequence of $Co(Cp)_2$/N_2/O_3/N_2. GPC is calculated using a linear regression of film thickness resulting from 50, 135, and 300 cycle depositions.

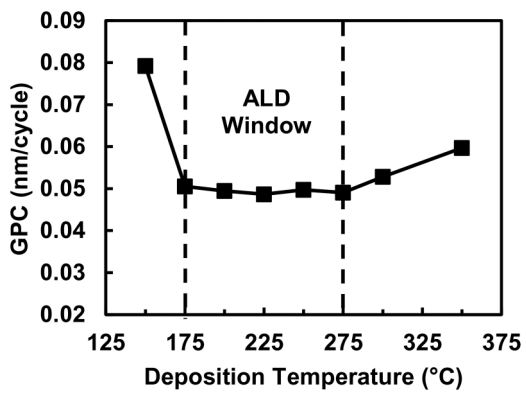

FIG. 1. GPC vs deposition temperature for the $Co(Cp)_2/O_3$ ALD process.

Film thickness is measured at the center of a 5 in. Si wafer. An ALD "temperature window" with a nearly constant GPC of approximately 0.05 nm/cycle is observed between a deposition temperature of 175 and 275 °C with GPC increasing both below and above this temperature range. Within the ALD window, saturating growth behavior is observed for greater than 0.1 s pulses of $Co(Cp)_2$ and greater than 3 s pulses of O_3.[28]

To examine nucleation and growth on various substrates for potential device applications, plots of film thickness versus ALD cycles are shown in Fig. 2 for (a) deposition at 150, 250, and 350 °C on Si and (b) for deposition at 250 °C on SiO_2/Si, and Co/Si substrates. On Si substrates at 250 °C, a linear fit indicates a GPC of ~0.05 nm/cycle with the *x* axis intercept indicating approximately zero nucleation delay. VASE modeling indicates that the thickness of the native SiO_2 layer does not change ($\Delta d_{SiO2} < \pm 1$ nm) during the ALD process, consistent with reports of O_3 oxidation of bare Si substrates at 200 and 300 °C.[29] The nucleation delay on Si was found to be negligible up to 275 °C. At temperatures above the ALD window, the nucleation delay increases to more than 20 cycles at 300 °C and more than 25 cycles at 350 °C. On a thermally grown SiO_2 surface, a lower GPC of 0.043 nm/cycle was found, again with no nucleation delay.

On Co metal [Fig. 2(b)], however, a much higher GPC of 0.21 nm/cycle is seen along with a positive *y* axis intercept of ~6.2 nm. Although part of the *y* axis intercept can be attributed to the presence of an initial thin ~1 nm native Co oxide,[30] it does not account for the enhanced growth rate. Additional 100 and 300 cycle depositions were therefore performed using *only* the O_3 pulses [the $Co(Cp)_2$ pulses are omitted from the ALD pulse sequence] and are shown in Fig. 2(b) as "x" symbols. It is seen that depositions with only O_3 cycles show nearly the same growth as with the full ALD cycles. Thus, it is clear that the enhanced growth rate and majority of the *y* axis intercept are not due to ALD, but rather to direct O_3 oxidation of the Co substrate.

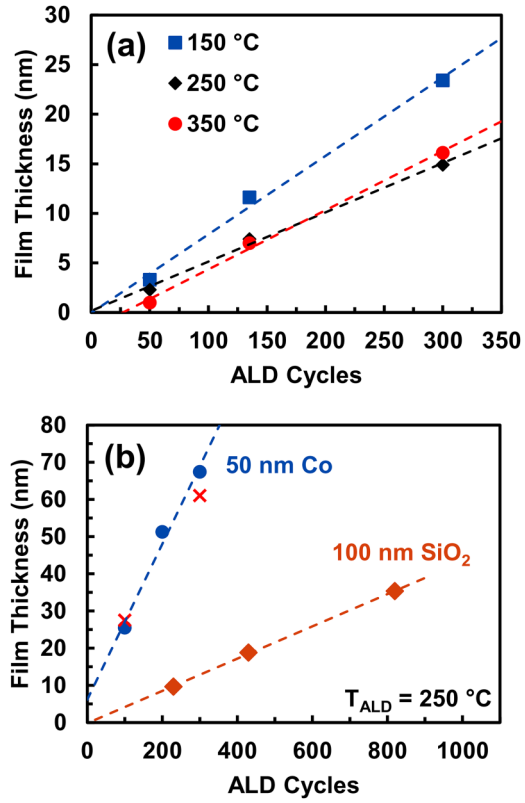

FIG. 2. ALD cobalt oxide film thickness as a function of ALD cycles on (a) Si and (b) SiO_2 and Co. Dashed lines are linear regression fits of the data. "x" symbols show growth data on Co using only O_3 pulses.

VASE film thickness uniformity maps across a 5 in. wafer are shown in Fig. 3 for deposition temperatures of 150, 250, and 350 °C, temperatures below, within, and above the ALD window, respectively. Film nonuniformity indicated is calculated as the percentage of standard deviation/average thickness. Film growth within the ALD window at 250 °C [Fig. 3(b)] is uniform (4.7% nonuniformity) and smooth (0.6 nm RMS roughness) across a 5 in. Si wafer. Outside the temperature window, nonuniformity increases significantly. Below the ALD window at 150 °C [Fig. 3(a)], the nonuniformity increases to 37% and overall thickness increases substantially (note different scales). A much thicker region is observed near the $Co(Cp)_2$ precursor inlet, strongly suggesting condensation of $Co(Cp)_2$. Above the ALD window at a deposition temperature of 350 °C [Fig. 3(c)], the nonuniformity is about 35%. There is a strong thickness gradient in the direction of the $Co(Cp)_2$ flow, with thicker film growth near the inlet than at 250 °C to thinner than 250 °C near the far edge of the wafer, consistent with thermal decomposition of the precursor. Note that due to the increase in nucleation delay at 350 °C, the thickness at the center of the wafer happens to be about the same as for the 250 °C deposition, as evident in Fig. 2(a).

B. Crystallinity and morphology

The crystallinity and phase of as-deposited films was analyzed by GIXRD. Shown in Fig. 4 are GIXRD scans performed on 3.3, 8.1, 12.6, and 19.7 nm thick films deposited on Si substrates at 250 °C (within the ALD temperature window). The detected peaks in the GIXRD spectra of all films correspond to randomly oriented polycrystalline cubic Co_3O_4. Although no peaks attributable to crystalline CoO are detected, the presence of *amorphous* CoO cannot be ruled out by XRD. The Co_3O_4 crystallite size (estimated from Scherrer formula) increases with film thickness, from roughly 4 nm crystallites for the thinnest film to roughly 11 nm for the thickest film. The increase in crystallite size with increasing thickness is consistent with earlier reports of ALD Co_3O_4.[6,22,24] Note that due to a computer control malfunction following a software update, the N_2 carrier gas flow rates were four times higher for the three thinner films in Fig. 4 [indicated with daggers (†)]. As the films grown using the 4× higher flow rates exhibit the same crystallographic peaks as the 19.7 nm thick film grown with the nominal flow rates, it appears the N_2 flow rate has no noticeable impact on crystallinity. Also shown in Fig. 4 is a GIXRD scan of a 23.4 nm thick film deposited at 150 °C (slightly below the ALD temperature window) and a 16.0 nm thick film deposited at 350 °C (well above the ALD temperature window). For both the 150 and 350 °C films, the Co_3O_4 phase is still observed with no peaks attributable to CoO. Compared with the 250 °C films, the 150 °C film shows the same but relatively weaker peaks, indicating smaller crystallites. For the 350 °C film, the peaks corresponding to the (220), (400), and (511) orientations are suppressed, while the intensity of the (111) and (440) orientations are relatively unchanged. These differences may be due to precursor decomposition, which can lead to incorporation of carbon that disrupts crystallization.

XPS was carried out on ~20 and 100 nm thick films deposited at 250 °C to assess carbon contamination. A 60 s Ar sputter clean of the surface was performed to remove adventitious carbon from the surface. Analysis of relative elemental concentrations indicates that carbon is below detection limits for both films. As Ar sputtering is known to reduce CoO_x, an accurate estimate of stoichiometry could not be obtained.[31]

C. Optical properties

Three samples grown at 250 °C using 100, 200, and 300 ALD cycles were measured via multisample analysis using the WVASE software suite. A 2 nm thick native SiO_2 layer was incorporated beneath the Co_3O_4 layer in the model for each of the films which provided a low value of mean-standard-error for the fit. A representative plot of R.I. and extinction coefficient, *k*, versus wavelength for as-deposited Co_3O_4 films is shown in Fig. 5(a). The films exhibit a value of R.I. of approximately 2.8 at 632.8 nm. Shown in Fig. 5(b) is a plot of R.I. versus deposition temperature for the series of 300 cycle films from Fig. 1. Within the ALD temperature window, R.I. is roughly constant at between 2.80 and 2.83, suggesting the film optical properties do not vary significantly within this temperature range.

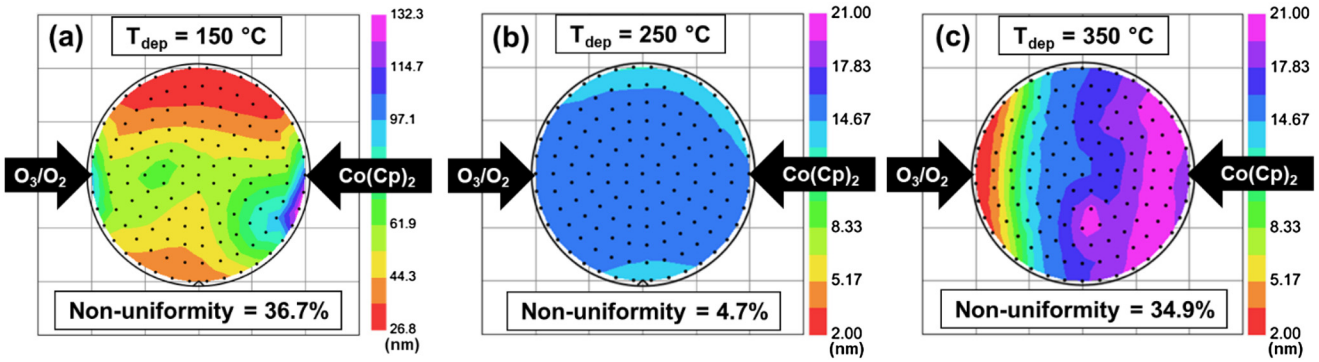

FIG. 3. VASE thickness maps of ALD cobalt oxide films grown on 5 in. Si wafers using 300 cycles at deposition temperatures of (a) 150, (b) 250, and (c) 350 °C. Precursor inlet and flow directions (arrows), deposition temperature, and nonuniformity are indicated.

The optical transitions, E_{opt}, of the Co_3O_4 films can be estimated from

$$(\alpha h\upsilon)^n \propto (h\upsilon - E_{opt}), \quad (1)$$

where α is the optical absorption at high frequency ($\alpha = 4\pi k/\lambda$), h is Planck's constant, υ is the frequency of incident light, and n can take different values depending on the types of electronic transitions ($n = 2$ for allowed direct transitions). Shown in Fig. 6 are Tauc plots of $(\alpha h\upsilon)^2$ versus $h\upsilon$ generated from the VASE multisample analysis. Direct E_{opt} are estimated by extrapolating the x axis intercept of linear regressions to the most linear regions. Three linear regions are identified yielding direct allowed optical transition estimates of $E_{opt1} = 0.76$ eV, $E_{opt2} = 1.50$ eV, and $E_{opt3} = 2.22$ eV. Shown in Fig. 6(c), E_{opt2} and E_{opt3} are stable throughout the ALD temperature window (note that E_{opt1} is not shown as the ellipsometer used for these measurements does not extend far enough into the infrared).

D. Electrical properties

Four-point probe measurements performed on an 88.5 nm thick sample deposited at 250 °C on 100 nm thermal SiO_2 substrates show resistivity in the range of 4.1–10.9 Ω cm.

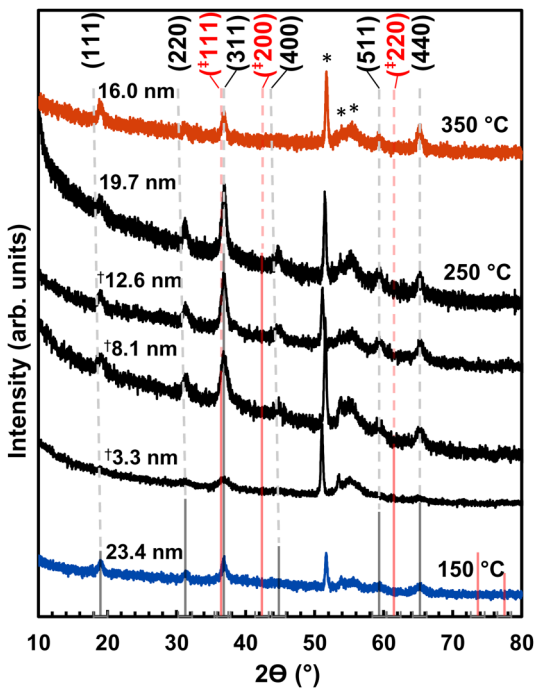

FIG. 4. GIXRD spectra for 3.3, 8.1, 12.6, and 19.7 nm ALD cobalt oxide films deposited at 250 °C, a 16.0 nm thick film deposited at 350 °C, and a 23.4 nm thick film deposited at 150 °C. Daggers (†) indicate films grown with 4× higher N_2 flow rates. Crystallographic orientations and relative intensities for randomly oriented cubic Co_3O_4 (XRD card 01-073-1701) and ‡CoO (card 01-071-1178) are shown as solid/dashed vertical lines. Stars (*) indicate peaks attributed to the underlying Si substrate.

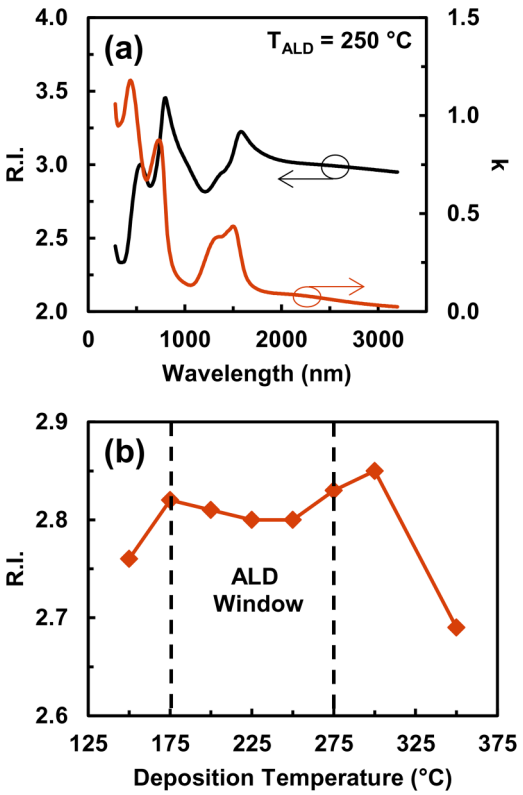

FIG. 5. (a) R.I. and k as a function of incident wavelength obtained from VASE multisample analysis on films grown at 250 °C using 100, 200, and 300 ALD cycles on Si substrates. (b) R.I. at 632.8 nm vs deposition temperature for the 300 cycle films from Fig. 1.

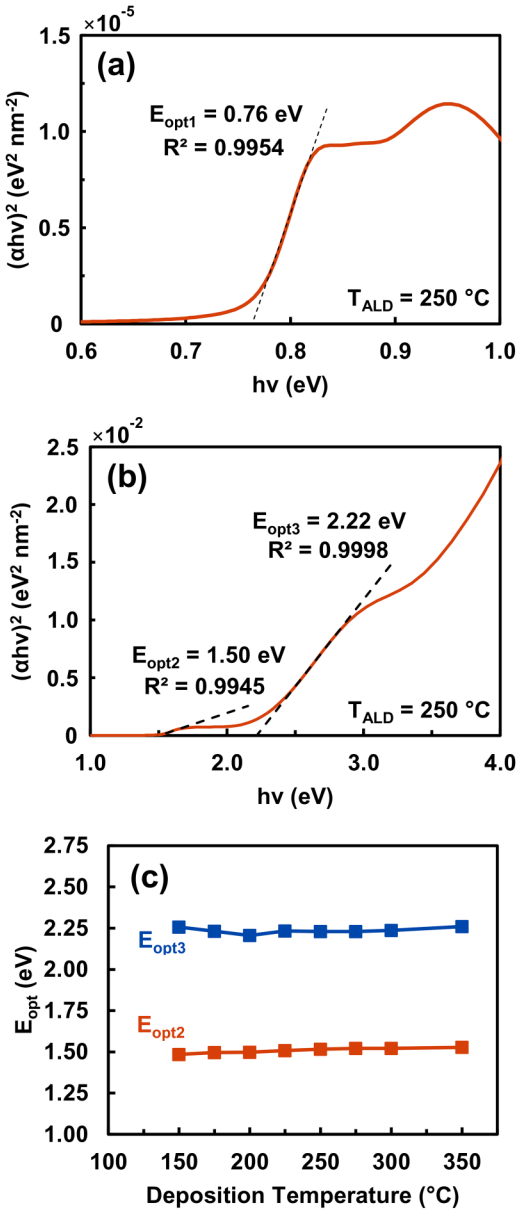

FIG. 6. (a) and (b) Tauc plots [$(\alpha h\nu)^2$ vs $h\nu$] generated from a multisample analysis of ALD Co_3O_4 films grown at 250 °C using 100, 200, and 300 cycles. Linear regressions (dashed lines) and estimated E_{opt} values are indicated. (c) Plot of E_{opt2} and E_{opt3} vs deposition temperature.

The resistivity range is lower than values reported for Co_3O_4 deposited via CVD (14.7 Ω cm)[11] and much lower than values reported for MOCVD (300–320 Ω cm)[10] and spray pyrolyzed Co_3O_4 (200 Ω cm or more than 10^3 Ω cm).[8,14] However, the resistivity obtained is roughly consistent with Co_3O_4 obtained via ALD using either $Co(Cp)_2$ and O_2 plasma (0.5–5.3 Ω cm)[18] or $Co(thd)_2$ and O_3 (0.1–4.5 Ω cm).[25] Despite the wide variation of resistivity values reported for Co_3O_4, all are well below the insulating CoO phase, which is reported as having a resistivity of ~10^{10} Ω cm.[32] Due to different processing and precursors, possible explanations for the variations in reported resistivity for Co_3O_4 films include differences in stoichiometry and impurities, crystal grain orientation and size, and film thickness. A mixed Co_3O_4/CoO phase might be expected to have a much higher resistivity, which could explain the high values reported for spray pyrolysis. Although the stoichiometry of our films was not precisely determined nor was it reported in the two previous ALD studies reporting resistivity, resistivities many orders of magnitude below the CoO phase suggest little if any CoO incorporation. Crystal orientation may also play a role in charge transport. For the thermal $Co(Cp)_2/O_3$ process reported here, the film is randomly oriented (Fig. 4), while the O_2 plasma process produced a (111) preferred orientation[18] and the $Co(thd)_2/O_3$ produced a (100) preferred orientation film.[25] Other properties such as thickness and crystal grain size can also have an effect. Whereas resistivity for the plasma ALD $Co(Cp)_2$ process was reported to be independent of film thickness, the minimum resistivity for the $Co(thd)_2/O_3$ process was for a film thickness of ~40 nm with both thinner and thicker films being more resistive. Larger grains are often associated with reduced resistivity. Klepper *et al.*,[12] however, reported that larger grains did not produce lower resistivity, interpreting this as transport taking place along grain boundaries. Cheng *et al.*[11] also found that mobility was not influenced by grain size and saw no impact of grain boundary scattering concluding that polaronic hopping of holes was responsible for charge transport at room temperature. Louardi *et al.*[14] reported that the conductivity of Co_3O_4 increased with temperature, consistent with a p-type semiconductor, and fit charge transport to variable range hopping.

E. Discussion

Table I contains a summary of ALD cobalt oxide processes to date that have reported an ALD temperature window (precursor, reactant, GPC, nucleation delay, and phase obtained, as well as R.I., optical transitions, and film resistivity if they were provided). [Note that although Ref. 13 reports an ALD process using bis(1,4-di-iso-propyl-1,4-diazabutadiene)cobalt and O_2, an ALD temperature window is not reported; the reported GPC is 0.808 nm/cycle (much greater than one monolayer/cycle), and growth does not appear to saturate with either precursor or reactant pulse time.] In this work, Co_3O_4 films were deposited using $Co(Cp)_2$ and O_3. A saturating growth rate of ~0.05 nm/cycle with a negligible nucleation delay on Si was observed within an ALD temperature window of 175–275 °C. There have been two earlier reports of ALD using $Co(Cp)_2$ and O_3.[22,23] Although these two reports agree roughly on the temperature range of the ALD window, they disagree on the GPC within the window and the relationship of GPC with temperature outside the ALD window. Comparing to our results, the GPC of 0.05 nm/cycle on Si found in this work within the ALD window of 175–275 °C is somewhat higher than that reported by both Diskus *et al.*,[22] who saw 0.045 nm/cycle on soda lime glass and 0.041 nm/cycle on Si (the authors indicate that the difference between substrates was likely due to the Si substrate being placed further in the reaction chamber from the inlet than the glass) and Huang *et al.*[23] who saw 0.037 nm/cycle on Si. On SiO_2, we see a slightly lower GPC

of 0.043 nm/cycle, lower than what we see for Si, which is opposite of Diskus *et al*. but might also be explained by the wafer positioning in the earlier work, as indicated by the authors.

At temperatures below the ALD window (<175 °C), we find that the GPC increases dramatically with decreasing temperature, opposite to both previous reports which showed decreasing growth.[22,23] The increase in GPC is accompanied by a dramatically increased nonuniformity (~37% at 150 °C), shown in Fig. 3(a), with decreasing thickness away from the $Co(Cp)_2$ inlet, suggesting condensation. Thus, the decrease in growth rate seen in previous reports could be due to positioning of the substrate further from the $Co(Cp)_2$ inlet so that much of the $Co(Cp)_2$ condenses on the chamber walls or precursor delivery lines before reaching the substrate.

At temperatures above the ALD window (>275 °C), we find that the GPC increases slowly with temperature, consistent with Huang *et al*., but opposite to Diskus *et al*. in which a decrease in growth rate was reported. As seen in Fig. 3(c), deposition is highly nonuniform (~35% at 350 °C) with a thicker region once again observed near the $Co(Cp)_2$ inlet and very little growth away from the $Co(Cp)_2$ inlet. The discrepancy with Diskus *et al*. is thus also likely due to the substantially nonuniform film growth at this temperature resulting from precursor decomposition and the position of the sample or measurement with respect to the $Co(Cp)_2$ inlet.

Considering nucleation delay on Si, we find that the number of nucleation cycles inside the temperature window is small (0 ± ~5 cycles), whereas at 300 °C (above the window), the number of nucleation cycles increases to more than 20. The apparent delay in growth at 300 °C and above could be due to desorption of species that play a role in the initial nucleation stages or due to consumption of precursor molecules resulting from decomposition near or possibly inside the $Co(Cp)_2$ inlet.

As for phase and composition, GIXRD spectra in Fig. 4 reveal the presence of Co_3O_4 at a deposition temperature of 250 °C, consistent with Diskus *et al*. who also detect the Co_3O_4 phase within the ALD window via XRD. Huang *et al*. report Co_3O_4 at 250 °C for thicker films. They did not report XRD data, but instead based this assessment on Raman spectroscopy for 100 nm thick films and x-ray photoelectron spectroscopy (XPS) for thinner films. For films less than 10 nm thick, they report the presence of mixed CoO/Co_3O_4.[23] They interpret their results as the morphology changing from mostly CoO at the initial growth stage to Co_3O_4 for thicker films, with the change to Co_3O_4 requiring thicker films with increasing deposition temperature. Diskus *et al*., on the other hand, detect CoO only in a mixed Co_3O_4/CoO phase and only above the ALD window at 331 °C.[22] As shown in Fig. 4, we are unable to detect the CoO phase using GIXRD in films down to 3.3 nm thick. We also do not detect the presence of CoO in films deposited at 350 °C or at 150 °C, above and below the ALD temperature window, respectively.

The value of R.I. for thin film Co_3O_4 has been reported in the range of 2.67 (Ref. 17) to 2.8 (Ref. 10) with R.I. ≈ 2.7 reported for bulk Co_3O_4 powder.[34] Bulk CoO, on the other hand, is reported as having a much lower R.I. of ~2.2 to ~2.3.[35,36] Thus, the R.I. = 2.8 we obtained for as-deposited films is also consistent with Co_3O_4 rather than CoO, even for thinner films. The decrease in R.I. observed outside of the ALD window [Fig. 5(b)] is consistent with reduced density and/or incorporation of organic residue from either condensed $Co(Cp)_2$ molecules at lower temperatures or products of decomposed $Co(Cp)_2$ at higher temperature. The slightly reduced R.I. at 350 and 150 °C is consistent with the reduced crystallinity but likely not due to the presence of the lower R.I. CoO phase, which is not detected by GIXRD (Fig. 4) or indicated by optical transitions.

From multisample VASE analysis, direct allowed optical transitions of 0.76, 1.50, and 2.22 eV are estimated. Although optical transitions have not been reported on pure ALD films, the 1.50 and 2.22 eV optical transitions are within the range of reported values for CVD,[11] pulsed CVD,[13] MOCVD,[10] pulsed laser deposited,[16] and spray pyrolyzed[8,14] thin film Co_3O_4. Despite increasing interest and work on this material, the electronic structure and optical bandgap of Co_3O_4 are not fully understood and are still under debate. For example, while the ~1.9–2.2 eV transition is often identified as the direct bandgap[11,13,15] and the ~1.4–1.5 eV transition has been suggested to be the acceptor level,[11] more recently, others have identified 0.74 to ~0.8 eV as the fundamental direct bandgap,[16] a result predicted by DFT calculations.[7,16] Our observation of the 0.76 eV transition is in agreement with the 0.74 eV reported for pulsed laser deposited Co_3O_4 and predicted by DFT calculations to be the direct fundamental bandgap,[7,16] but does not rule out a larger bandgap. Finally, note that the observed transitions are all below the insulating CoO phase which is reported as having a bandgap in the range of 2.5–6.0 eV.[2–4]

IV. SUMMARY AND CONCLUSIONS

The electrical, optical, and structural properties of cobalt oxide thin films deposited via ALD using $Co(Cp)_2$ and O_3 are investigated. To date, these properties have not been widely reported for ALD cobalt oxide films. Uniform, saturating growth of ~0.05 nm/cycle with a negligible nucleation delay within an ALD temperature window of 175–275 °C was obtained over a 5 in. Si wafer. Both growth rate and nonuniformity increase both above and below the ALD window. From GIXRD, it is found that as-deposited films are cubic Co_3O_4. No evidence is found for the polycrystalline CoO phase, and the measured refractive index, optical transitions, and resistivity are all consistent with Co_3O_4. Spectroscopic ellipsometry measurements indicate a refractive index of 2.8, consistent with the 2.67–2.8 reported for Co_3O_4 but well above the 2.2–2.3 reported for CoO. Measured optical transitions of 0.76, 1.50, and 2.22 eV are all consistent with Co_3O_4 but below the 2.5–6 eV transitions reported for CoO. The 0.76 eV transition appears to support earlier experimental work and DFT calculations that point to a fundamental bandgap of 0.74 eV for Co_3O_4. From four-point probe measurements, resistivity in the range of 4.1–10.9 Ω cm is obtained, consistent with the p-type semiconducting Co_3O_4

phase but well below the $10^{10}\,\Omega\,cm$ reported for the insulating CoO phase.

Overall, our results indicate that ALD using $Co(Cp)_2$ and O_3 is promising for renewable energy applications requiring uniform deposition of a high-quality p-type semiconducting Co_3O_4, although the use of O_3 may rule out deposition on metal electrodes such as Co where oxidation dominated growth was observed.

ACKNOWLEDGMENTS

The authors thank Chris Tasker for equipment support, Ron Synowicki at J. A. Woollam Co., Lincoln, NE, for VASE multisample measurements, Dennis Hausmann and Paul Lemaire at Lam Research Corp., Tom Polson at EMD Performance Materials for XPS measurements, and RedWave Energy Inc. for financial support. This work was conducted at the Materials Synthesis and Characterization (MaSC) Center, a National Nanotechnology Coordinated Infrastructure (NNCI) Northwest Nanotechnology Infrastructure (NWNI) user facility at the Oregon State University, which is supported in part by the National Science Foundation (NSF) (Grant No. ECC-1542101) and Oregon State University.

[1]T. S. Tripathi and M. Karppinen, Adv. Mater. Interfaces **4**, 1700300 (2017).
[2]Z.-X. Shen *et al.*, Phys. Rev. B **42**, 1817 (1990).
[3]L. Liao *et al.*, Nat. Nanotechnol. **9**, 69 (2014).
[4]A. U. Mane and S. A. Shivashankar, J. Cryst. Growth **254**, 368 (2003).
[5]S. B. Herner, A. D. Weerakkody, A. Belkadi, and G. Moddel, Appl. Phys. Lett. **110**, 223901 (2017).
[6]J. Kim *et al.*, Chem. Mater. **29**, 5796 (2017).
[7]V. Singh, M. Kosa, K. Majhi, and D. T. Major, J. Chem. Theory Comput. **11**, 64 (2015).
[8]P. S. Patil, L. D. Kadam, and C. D. Lokhande, Thin Solid Films **272**, 29 (1996).
[9]E. Fischer Rivera, B. Atakan, and K. Kohse-Höinghaus, J. Phys. IV **11**, Pr3-630 (2001).
[10]A. Gulino, G. Fiorito, and I. Fragalà, J. Mater. Chem. **13**, 861 (2003).
[11]C.-S. Cheng, M. Serizawa, H. Sakata, and T. Hirayama, Mater. Chem. Phys. **53**, 225 (1998).
[12]K. B. Klepper, O. Nilsen, and H. Fjellvåg, J. Cryst. Growth **307**, 457 (2007).
[13]S. Jung, D. K. Nandi, S. Yeo, H. Kim, Y. Jang, J.-S. Bae, T. E. Hong, and S.-H. Kim, Surf. Coat. Technol. **337**, 404 (2018).
[14]A. Louardi, A. Rmili, T. Chtouki, B. Elidrissi, H. Erguig, A. E. Bachiri, K. Ammous, and H. Mejbri, J. Mater. Environ. Sci. **8**, 485 (2017).
[15]D. Barreca, C. Massignan, S. Daolio, M. Fabrizio, C. Piccirillo, L. Armelao, and E. Tondello, Chem. Mater. **13**, 588 (2001).
[16]L. Qiao *et al.*, J. Mater. Chem. C **1**, 4628 (2013).
[17]B. Han, K. H. Choi, K. Park, W. S. Han, and W.-J. Lee, Electrochem. Solid-State Lett. **15**, D14 (2011).
[18]M. E. Donders, H. C. M. Knoops, W. M. M. Kessels, and P. H. L. Notten, J. Electrochem. Soc. **158**, G92 (2011).
[19]V. Patil, P. Joshi, M. Chougule, and S. Sen, Soft Nanosci. Lett. **2**, 1 (2012).
[20]B. Han, K. Ha Choi, J. Min Park, J. Woo Park, J. Jung, and W.-J. Lee, J. Vac. Sci. Technol. A **31**, 01A145 (2013).
[21]B. Han, J.-M. Park, K. H. Choi, W.-K. Lim, T. R. Mayangsari, W. Koh, and W.-J. Lee, Thin Solid Films **589**, 718 (2015).
[22]M. Diskus, O. Nilsen, and H. Fjellvåg, Chem. Vap. Deposition **17**, 135 (2011).
[23]B. Huang, K. Cao, X. Liu, L. Qian, B. Shan, and R. Chen, RSC Adv. **5**, 71816 (2015).
[24]M. Rooth, E. Lindahl, and A. Hårsta, Chem. Vap. Deposition **12**, 209 (2006).
[25]K. B. Klepper, O. Nilsen, and H. Fjellvåg, Thin Solid Films **515**, 7772 (2007).
[26]M. Büyükyazi, T. Fischer, P. Yu, M. Coll, and S. Mathur, Dalton Trans. **46**, 12996 (2017).
[27]M. T. Vieyra-Eusebio and A. Rojas, J. Chem. Eng. Data **56**, 5008 (2011).
[28]K. E. K. Holden, M. A. Jenkins, and J. F. Conley, Jr., ECS Trans. **85**, 735 (2018).
[29]Z. Cui, J. M. Madsen, and C. G. Takoudis, J. Appl. Phys. **87**, 8181 (2000).
[30]H. G. Tompkins and J. A. Augis, Oxid. Met. **16**, 355 (1981).
[31]D. F. Mitchell, G. I. Sproule, and M. J. Graham, Surf. Interface Anal. **15**, 487 (1990).
[32]G. M. Joshi, M. Pai, H. R. Harrison, C. J. Sandberg, R. Aragón, and J. M. Honig, Mater. Res. Bull. **15**, 1575 (1980).
[33]M. E. Donders, H. C. M. Knoops, W. M. M. Kessels, and P. H. L. Notten, J. Power Sources **203**, 72 (2012).
[34]J. W. D. Martens, W. L. Peeters, H. M. van Noort, and M. Erman, J. Phys. Chem. Solids **46**, 411 (1985).
[35]R. J. Powell and W. E. Spicer, Phys. Rev. B **2**, 2182 (1970).
[36]D. Gallant, M. Pézolet, and S. Simard, J. Phys. Chem. B **110**, 6871 (2006).